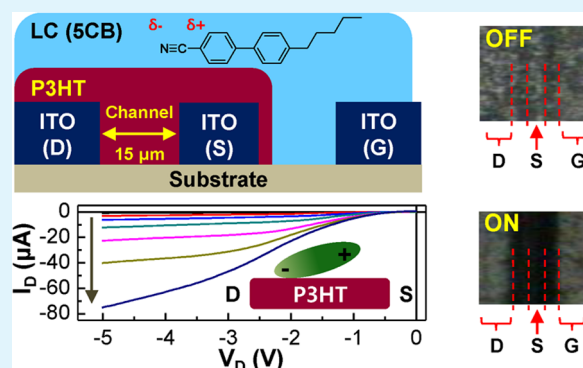# Liquid Crystal-Gated-Organic Field-Effect Transistors with In-Plane Drain−Source−Gate Electrode Structure

Jooyeok Seo,[†] Sungho Nam,[†] Jaehoon Jeong,[†] Chulyeon Lee,[†] Hwajeong Kim,*,[†,‡] and Youngkyoo Kim*

[†]Organic Nanoelectronics Laboratory, Department of Chemical Engineering, and [‡]Research Institute of Advanced Energy Technology, Kyungpook National University, Daegu 702-701, Republic of Korea

S *Supporting Information*

ABSTRACT: We report planar liquid crystal-gated-organic field-effect transistors (LC-*g*-OFETs) with a simple in-plane drain−source−gate electrode structure, which can be cost-effectively prepared by typical photolithography/etching processes. The LC-*g*-OFET devices were fabricated by forming the LC layer (4-cyano-4′-pentylbiphenyl, 5CB) on top of the channel layer (poly(3-hexylthiophene), P3HT) that was spin-coated on the patterned indium−tin oxide (ITO)-coated glass substrates. The LC-*g*-OFET devices showed p-type transistor characteristics, while a current saturation behavior in the output curves was achieved for the 50−150 nm-thick P3HT (channel) layers. A prospective on/off ratio (>1 × 10³) was obtained regardless of the P3HT thickness, whereas the resulting hole mobility (0.5−1.1 cm²/(V s)) at a linear regime was dependent on the P3HT thickness. The tilted ordering of 5CB at the LC-P3HT interfaces, which is induced by the gate electric field, has been proposed as a core point of working mechanism for the present LC-*g*-OFETs.

KEYWORDS: *liquid crystal, organic transistor, dipole, LC-g-OFET, 5CB*

1. INTRODUCTION

Organic field-effect transistors (OFETs) have recently attracted keen interest because of their potential for low-cost fabrication of plastic logic devices and flexible display backplanes.[1−4] The highest mobility of OFETs has reached 30−45 cm²/(V s) by employing organic single crystals,[5,6] but these values are still far behind the outstanding mobility (200−1160 cm²/(V s)) of inorganic FETs with highly crystalline inorganic materials.[7,8] Although organic semiconducting materials play a primary role in achieving high mobilities, gate insulating materials do also significantly influence on the practical performances of OFETs because the mobility of OFETs is sensitive to the amount of charges generated inside organic semiconducting layers (channel) by the electric field applied between gate and source electrodes.

Various materials, to date, have been used as a gate insulator for OFETs. One of the most representative materials is silicon oxide (SiOx), which is grown natively on doped silicon wafers and typically used for inorganic FETs due to its low dielectric constant ($\varepsilon \approx 3$).[9,10] However, the SiOx gate insulator requires high temperature processes (≫150 °C) for a defect-free dense layer so that it cannot be applied for OFETs at a commercial stage. On this account, several polymeric materials have been introduced as an organic gate insulator.[11−15] In particular, electrically insulating polymers with high dielectric constants, such as poly(vinylidene fluoride-*co*-trifluoroethylene-*co*-chlorofluoroethylene) (P(VDF-TrFE-CFE)), poly(4-vinylphenol)

cross-linked with 4,4′-(hexafluoroisopropylidene)diphthalic anhydride (PVP-HAD), and cyanoethylated poly(vinyl alcohol) (CR-V), contributed to achieving high mobilities because of the efficient charge formation in organic semiconducting layers by their dipole effect.[16−18] However, liquid crystals (LCs) have not been used as a gate insulator, even though they have considerably high dielectric constants[19] and possess huge potential for soft electronics that can mimic human bodies leading to humanoid robots, except our very recent quick report that focused on touch sensor applications but did not contain the fundamental aspect of transistor operation.[20]

In this work, we attempted to investigate the detailed operation principle of LC-gated-OFETs by varying the thickness of channel layer that directly contacts the LC gate insulator. A well-known representative nematic LC, 4-cyano-4′-pentylbiphenyl (5CB) (crystalline-to-nematic transition temperature = 18 °C; nematic-to-isotropic transition temperature = 35 °C), was used as the LC layer, while poly(3-hexylthiophene) (P3HT) was employed as the channel layer. A simple in-plane drain-source-gate (D-S-G) electrode structure, leading to a planar device, was made by employing typical photolithography/etching processes of indium−tin oxide (ITO) that has good adhesion property for semiconducting

polymer films upon wet-coating. The resulting OFETs have a geometry of bottom source/drain electrodes and top LC gate insulator that is controlled by the gate electrode next to the source electrode. The top and bottom surfaces of the channel layer (P3HT) contact the LC layer and the ITO source/drain electrodes, respectively, whereas the end part of the LC layer is directly connected to the gate electrode (see Figure 1a). Hence
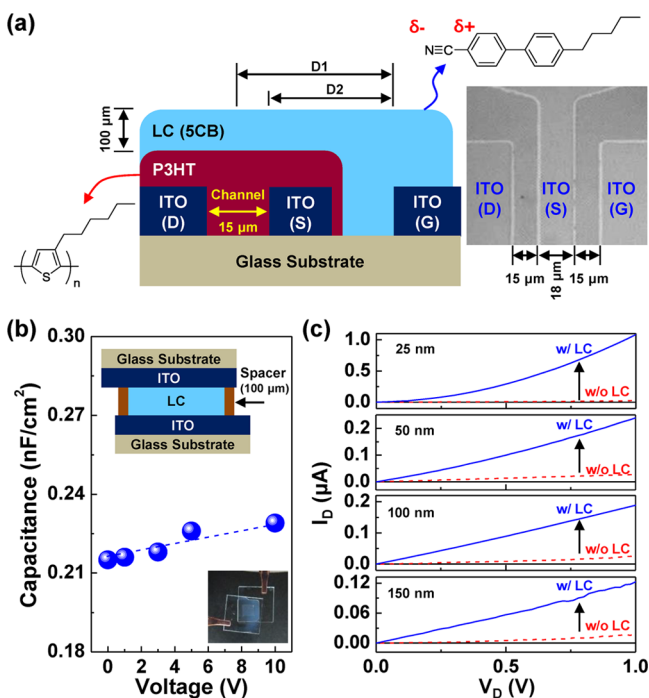

Figure 1. (a) Illustration for the device structure of LC-*g*-OFET (right: optical microscope image for the patterned ITO-glass substrate) and the chemical structure of 5CB and P3HT (note that the P3HT layer is not linked to the gate electrode, see Figure S1 in the Supporting Information). (b) Capacitance (frequency = 1 kHz) as a function of voltage for the ITO/LC(5CB)/ITO structure (insets: cross-section structure and top-view image). (c) Current (I_D)–voltage (V_D) characteristics of devices with (w/) and without (w/o) the LC layer on the P3HT layer at $V_G = 0$ V; the P3HT thickness is given on each graph.

we named the present OFET structure "planar LC-gated-OFET (LC-*g*-OFET)", which has a merit of simple device structure, leading to easy and low-cost fabrications, and is useful for various soft electronic devices including ultrasensitive tactile sensors, soft biomedical devices for diagnosis, flexible pressure sensors, flexible wearable touch sensors, etc.

2. RESULTS AND DISCUSSION

As shown in Figure 1, the thickness of the LC layer was controlled to be 100 μm, whereas the channel length between the source electrode and the drain electrode was fixed as 15 μm (see Figure 1). First, we examined the capacitance of the 100 μm thick LC (5CB) layer and the channel current change by the presence of the 5CB layer on the channel (P3HT) layers with four different thicknesses. As shown in Figure 1b, the capacitance of 5CB in the ITO/5CB/ITO structure was gradually increased as the applied voltage increased (frequency = 1 kHz), which does indirectly reflect the high dielectric feature of 5CB [dipole moment = 2.58 D, dielectric constant = 18 (nematic) and 11 (isotropic)]. Interestingly, when the 5CB

layer was placed on the channel layer without applying any gate voltage ($V_G = 0$ V), a huge jump in the drain current (I_D) was measured between the source electrode and the drain electrode regardless of the P3HT thickness (Figure 1c). In addition, the current jump became larger as the drain voltage (V_D) increased. This phenomenon can be attributed to the formation of charges in the channel layer by the strong dipole effect of 5CB.[19,21] Interestingly, the degree of current jump was much more pronounced for 25 nm than other thicknesses, reflecting that the thinnest (25 nm) P3HT layer has the highest ratio of the volume affected by the LC dipole to the unaffected (neutral) volume in the P3HT layer.

To know the influence of V_G on the channel current of devices, we measured output curves by varying V_G from 0 V to −60 V (note that the P3HT layer was removed from the S-G zone and the gate electrode in order to prevent possible leakage currents between the source electrode and the gate electrode, see Figure S1 in the Supporting Information). As V_D increased negatively at a fixed V_G, I_D was significantly increased irrespective of the P3HT thickness (see Figure 2a). This result indicates that the present devices are p-type (we note that the devices did not work under n-type operation by setting positive V_G and V_D). In the case of the 25 nm thick P3HT layer, a slight
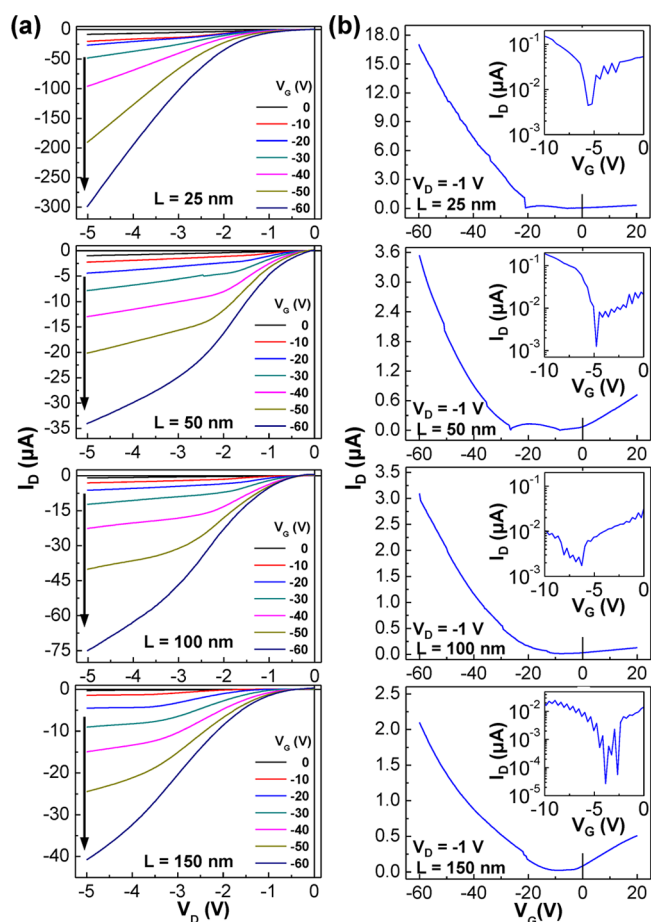

Figure 2. (a) Output and (b) transfer curves of LC-*g*-OFETs according to the thickness of the channel (P3HT) layer. V_G was varied from 0 to −60 V for the measurement of output curves, whereas V_D was fixed as −1 V for the measurement of transfer curves (linear regime). The on/off ratio ($R_{ON/OFF}$) was ~4 × 10³ (25 nm), ~3 × 10³ (50 nm), ~2 × 10³ (100 nm), and ~5 × 10³ (150 nm) (see the off current parts in the insets in b).

saturation behavior in the output curves was measured at a low V_G (−10 V and −20 V) but almost no saturation was measured when V_G was further increased at the given V_D range. Despite there being almost no saturation for the 25 nm thick P3HT layer, the highest I_D (ca. −300 μA) was measured at the same V_G (−60 V). This result (no saturation but high current) can be assigned to the overcharged channel layer by the strong LC dipole effect because of the limited channel volume (the thinnest P3HT layer here).[22] Interestingly, the 50 nm thick P3HT layer delivered an obvious saturation shape over the wide V_G range in the output curves. A similar saturation shape was measured for the 100 nm thick P3HT layer at the V_D range up to −5 V, which showed higher I_D values than the 50 nm thick P3HT layer at the same V_G. The device with the 150 nm thick P3HT layer did also show the saturation behavior but the I_D value was rather reduced compared to the device with the 100 nm thick P3HT layer. This result implies that 150 nm is too thick to effectively form the positively charged zone close to the S/D electrodes.[22]

Next, the transfer curves measured at V_D = −1 V (linear regime) are intensively discussed in order to equally compare all devices. We note that the saturation mobility (see Table S1 in the Supporting Information) could be obtained for three thicknesses, except 25 nm (no saturation current), when V_D was increased up to −30 V in order to meet the saturation regime condition ($V_D > V_G - V_{TH}$).[22] As shown in Figure 2b, a noticeable transfer curve was obtained from all devices although the shape was slightly different each other. A particular attention is paid to the quite high (negatively) threshold voltages (V_{TH}) for all devices. Taking into account the high dielectric constant of 5CB, I_D is considered to quickly increase with V_G. However, as observed from the transfer curves, the turn-on state seems to be delayed until V_G reaches ca. −15 V to −20 V depending on the thickness. This phenomenon is considered as the result of the far distance between the channel region and the gate electrode (see D1 = 40.5 μm in Figure 1a), which is considerably a large value compared to the typical thickness of gate insulating layers (300−700 nm).[11−24] In this regard, the turn-on voltage (i.e., V_{TH}) is expected to be further decreased by controlling the distance between the channel region and the gate electrode. Despite such disadvantage, the on/off ratio reached ~4 × 10³ for 25 nm and ~5 × 10³ for 150 nm (note that more than 1 × 10³ was also achieved for other two middle thicknesses).

To calculate the hole mobility from the transfer curves in Figure 2b, we assumed that the distance between the gate electrode and the channel layer corresponded to the thickness of the gate insulating layer because the 5CB molecules were uniformly connected with the constant thickness (100 μm) between the gate electrode and the channel layer. In other words, we can imagine that the gate electrode is moved on top of the LC layer with keeping the distances (D1 or D2) in Figure 1a, leading to a typical transistor geometry with a top gate electrode, so that the hole mobility of the present LC-g-OFET devices can be reasonably calculated by applying mobility equations used for conventional FET structures.[25] On the basis of this reasonable assumption, the hole mobility (μ_h) of devices was calculated using $I_D = (W/L)\mu_h C_i[(V_G - V_{TH})V_D - (V_D^2/2)]$ in a linear regime ($V_D < V_G - V_{TH}$), where W, L, and C_i are the channel width, the channel length, and the capacitance of gate insulator, respectively. As shown in Figure 3, the hole mobility reached ~1.1 cm²/(V s) (D1) and ~0.9 cm²/(V s) (D2) for the 25 nm thick P3HT layer, which approaches
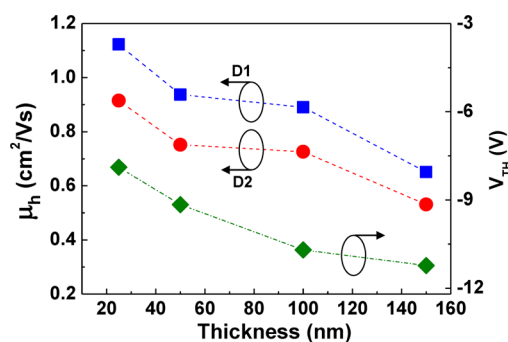

Figure 3. Hole mobility (μ_h) and threshold voltage (V_{TH}) of LC-g-OFETs as a function of the thickness of the channel (P3HT) layer (note that these data were extracted from the transfer curves in Figure 2b). Two different dimensions (see D1 and D2 in Figure 1) were used to calculate the capacitance (C_i) of the 5CB gate insulator in the present device structure because the LC layer was connected to the channel area from the gate electrode in a planar geometry.

the highest values reported for the OFETs with the P3HT channel layer (linear regime: 3.4 cm²/(V s), saturation regime: 2.5 cm²/(V s)).[26] However, the hole mobility was gradually decreased as the P3HT thickness increased, which is in accordance with the V_{TH} trend. The gradual decrease in the hole mobility can be basically attributed to the increased contact resistance because of the increased P3HT thickness. In addition, it is also considered that the charge transport (linear regime) in the present planar LC-g-OFET devices is strongly dependent on the effective amount (ratio) of charges (holes) per thickness, which are generated in the channel layer, as discussed in the output curves (see Figure 2a). Here the origin of V_{TH} (i.e., turn-on) in the present planar LC-g-OFETs can be attributed basically to the dipole alignment of 5CB which might be maximized by increasing the (gate) electric fields (see also Figure 4). However, as discussed above, the V_{TH} values in the present planar device geometry were relatively high compared to the drain voltages because of the far distance between the channel region and the gate electrode (see Table S1 in the Supporting Information).

To understand the working mechanism of planar LC-g-OFETs, we measured polarized optical microscope (POM) images by changing a polarization angle. As shown in Figure 4, a gray color was measured under linear polarization (0°) even at no bias condition, while no perfect dark (black) state was measured under cross-polarization (90°). This result implies that the 5CB molecules made a tilted homeotropic alignment on top of the P3HT layer at no bias condition as illustrated in Figure 4a. However, when V_D = −1 V was applied (only drain bias), the channel (D-S interelectrode) area between the drain electrode and the source electrode became slightly darker under linear polarization and much darker under cross-polarization (see "1" in Figure 4b). The similar darkening phenomenon under linear and cross-polarizations was observed for the S-G interelectrode area (between the source electrode and the gate electrode) when V_G = −15 V was applied (only gate bias) (see Figure 4c). These results indicate that only V_D = −1 V or V_G = −15 V could change the alignment of 5CB molecules from the tilted homeotropic state to the tilted in-plane state but the alignment (top view) was not perfect and quite tilted from the direction parallel to the D-S-G electrodes (note that the dipole direction is opposite according to the polarity of electrodes in Figure 4bc). Surprisingly, when V_G was increased up to −60 V,
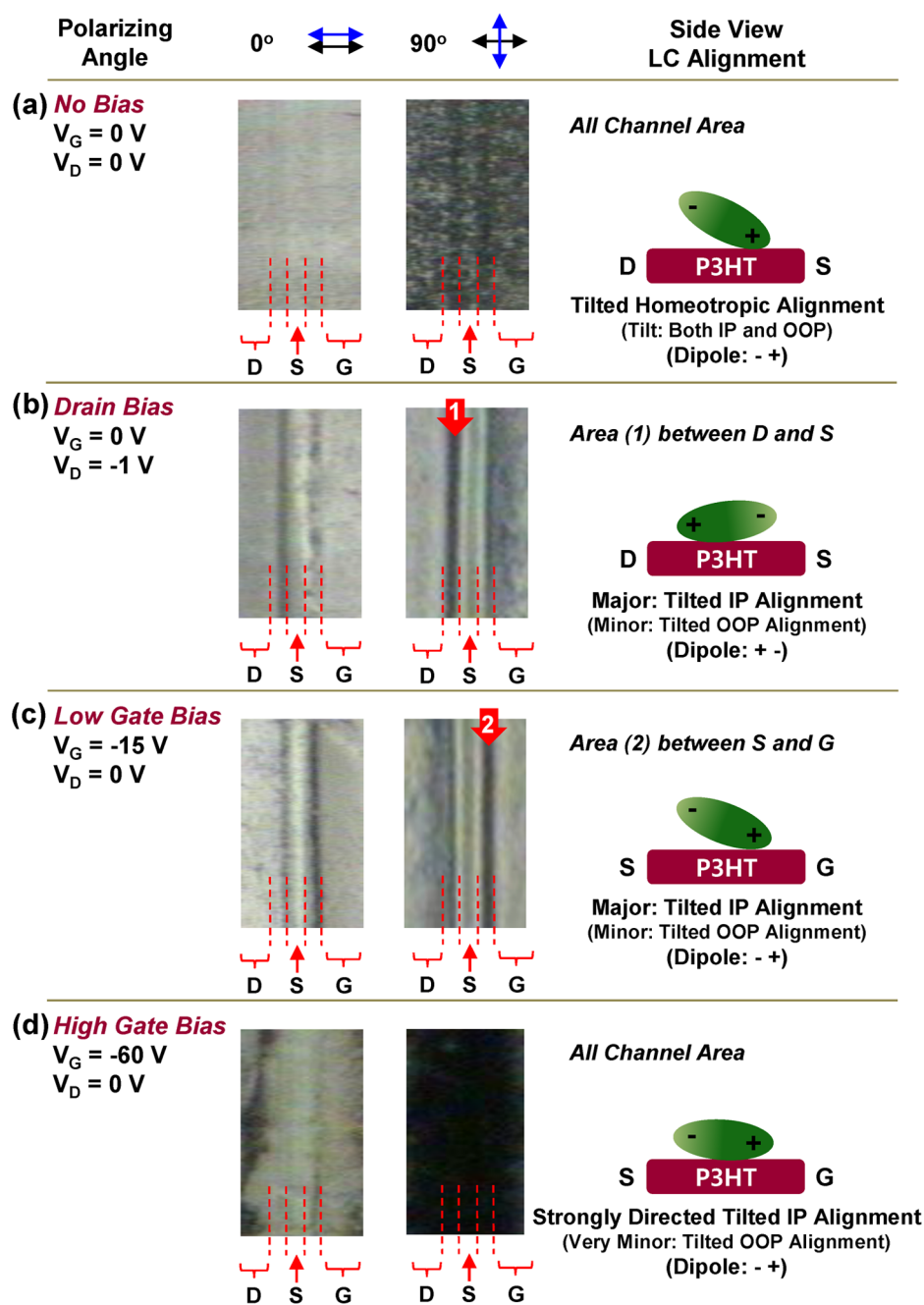
Figure 4. Optical microscope images for the LC-*g*-OFET device (P3HT thickness = 100 nm) according to the four different combinations of gate (V_G) and drain (V_D) voltages: The polarizing angles between top and bottom polarizers are given on top of the images. The possible alignment of LC (5CB) on the P3HT layer is illustrated on the right part of each optical image.

the whole channel area (including its vicinity area) between the drain electrode and the gate electrode became extremely dark under cross-polarization (gray under linear polarization). This reflects that most of 5CB molecules in the whole channel area made a strongly directed (but slightly tilted) in-plane alignment with the well-ordered 5CB dipoles parallel to the D-S-G electrode direction. Hence it is obvious that the high gate bias does indeed govern the LC (5CB) alignment in the present planar device structure.

In addition to the LC alignment study by separately applying either V_D or V_G (Figure 4), we tried to investigate the LC alignment by applying both V_D and V_G at the same time and by changing the polarization angles step by step. As shown in

Figure 5a, the brightness of images was decreased gradually as the polarization angle increased up to 90° without any unexpected brightness change at a particular angle, which reconfirms the tilted homeotropic alignment of 5CB molecules as illustrated in Figure 5b (top) at no bias condition (see Figure 4). When $V_G = -15$ V and $V_D = -1$ V were applied, both the channel area and the S-G interelectrode area became gradually dark as the polarization angle increased up to 90° but were not perfectly dark even at 90°. Therefore, it is considered that $V_G = -15$ V in the presence of $V_D = -1$ V is insufficient to govern whole parts of the channel area leading to a flip of 5CB dipoles form $(+ -)$ to $(- +)$ directions (see discussion in Figure 4). However, when $V_G = -60$ V and $V_D = -1$ V were applied, the
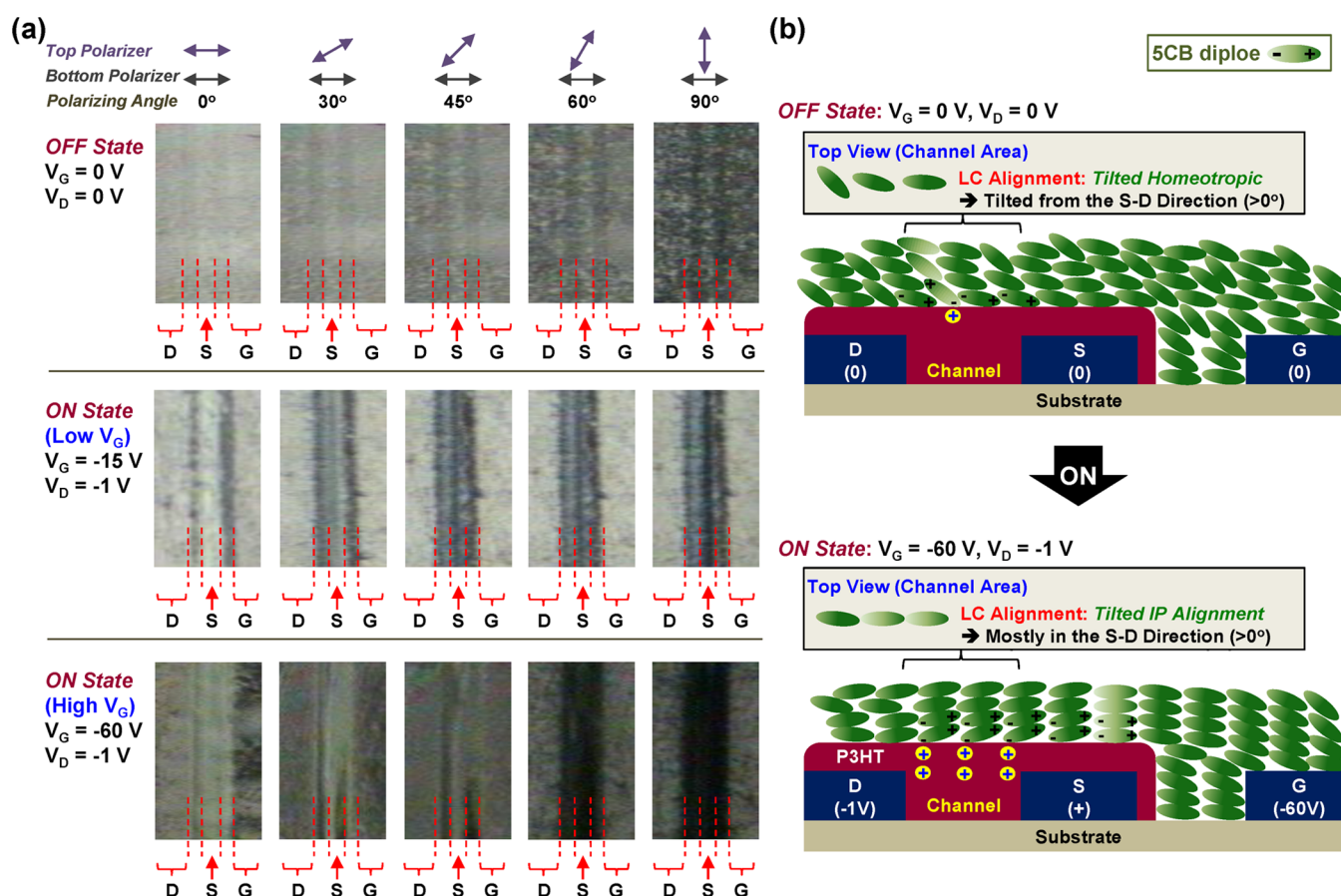
Figure 5. (a) Optical microscope images for the LC-*g*-OFET device (P3HT thickness = 100 nm) according to the three different combinations of gate (V_G) and drain (V_D) voltages with respect to the polarizing angles which are given on top of (a). (b) Proposed LC alignment for the operation of LC-*g*-OFETs: (top) Off-state ($V_D = 0$ V and $V_G = 0$ V) leading to a tilted homeotropic alignment, (bottom) On-state ($V_D = -1$ V and $V_G = -60$ V) leading to a tilted in-plane (IP) alignment. We note that the P3HT layer was not linked to the gate electrode (see Figure S1 in the Supporting Information).

channel area became further dark (but not absolutely black as explained in Figure S2 in the Supporting Information) under cross-polarization, compared to the vicinity area of which color was still dark gray. Hence most of 5CB molecules in the channel area under high gate bias condition are supposed to be aligned parallel to the direction of D-S-G electrodes, but some of them are considered to be still slightly tilted in the in-plane and out-of-plane direction of the P3HT film (layer) as illustrated in Figure 5b (bottom). However, the 5CB molecules in the vicinity area, apart from the channel area, did still follow the tilted hemeotropic alignment, even though the degree of homeotropic state was relatively weakened because of the less brightness at $V_G = -60$ V than $V_G = -15$ V. On the basis of these LC alignment study, we can clearly picture the alignment of 5CB molecules in the channel area at the on state (Figure 5b (bottom)), in which the negative end of dipole is considered to induce the positive charges in the P3HT layer. Here we note that the dipole direction in the channel (D-S interelectrode) area between the drain electrode and the source electrode was flipped from ($-$ + at $V_D = -1$ V and $V_G = -15$ V) to (+ $-$ at $V_D = -1$ V and $V_G = -60$ V) by the strong gate bias (-60 V) that overwhelms the weak drain voltage (-1 V) (see video clips in Figure S3 in the Supporting Information).

3. CONCLUSION

The planar LC-*g*-OFET devices, which consist of the in-plane aligned drain-source-gate electrodes, were fabricated by forming the 100 μm thick LC (5CB) layers on the P3HT channel layers. The channel current, even at no gate bias condition, was noticeably sensitive to the P3HT thickness when the LC layer was just placed on top of the P3HT layer. The present LC-*g*-OFET devices showed p-type transistor characteristics, proving that the LC layer did successfully act as a gate insulator in the planar electrode geometry. In particular, the highest drain current (max. 300 μA) was obtained for the planar LC-*g*-OFET device with the thinnest (25 nm) P3HT layer due to the closest distance of the charged zone to the S/D electrodes at the expense of current saturation behavior. As the P3HT thickness increased from 25 nm, all devices exhibited current saturation trends in the output curves, which evidence the presence of depletion zone as observed for typical gate insulators. The planar LC-*g*-OFET devices exhibited an encouraging hole mobility of 0.5−1.1 cm^2/(V s), which was dependent on the P3HT thickness. The core operation mechanism of the planar LC-*g*-OFET devices has been assigned to the tilted in-plane alignment and dipole flip (after V_{TH}) of 5CB molecules at the LC-P3HT interfaces by the increased gate voltage, which enables the negative end of 5CB dipole to approach the surface of the P3HT layer leading to generating more positive charges in the channel layer. Finally, the basic concept of the present

planar LC-*g*-OFET devices is expected to be widely applied for various applications, such as ultrasensitive tactile sensors, biomedical sensory devices, advanced optical devices, mesophase-logic devices for humanoid robots, etc., by further optimization of device structures, when it comes to their simple fabrication processes but powerful performances.

4. EXPERIMENTAL SECTION

Materials and Device Fabrcaton. 5CB (purity = 98%) and P3HT (weight-average molecular weight = 30 kDa, polydispersity index = 1.7, regioregularity = 97%) were supplied from Sigma-Aldrich and Rieke Metals, respectively. The P3HT powder was dissolved in toluene at a solid concentration of 15−30 mg/mL, whereas ITO-glass substrates were patterned to make planar drain-source-gate electrodes. The channel length between the source and drain electrode was 15 μm (see Figure 1a). On top of the cleaned ITO-glass substrates, the P3HT films were spin-coated to make a channel layer and annealed for 30 min at 120 °C (P3HT thickness = 25, 50, 100, and 150 nm). The thickness of P3HT layers and electrodes was measured using a surface profiler (alpha-step 200, Tencor). To prevent a possible leakage current between the source electrode and the gate electrode, the P3HT layer was removed from the S-G zone and the gate electrode using a speicalized nano/micropositioning stage with a sharp scribing tool (see Figure S1 in the Supporting Information). Poly(ethylene terephthalate) (PET) film (thickness = 100 μm), which has a rectangular hole in its center, was mounted on the P3HT layer. Then 5CB was filled inside the rectangular hole and another PET film (without any hole) or a slide glass was placed on top of the 5CB-filled PET bank to control the thickness (100 μm) of the LC (5CB) layer.

Measurements. The capacitance of the 100 μm thick 5CB layer (see insets in Figure 1b) was measured using an impedance analyzer (VersaSTAT 4, Princeton Applied Research), while a specialized OFET measurement system equipped with a semiconductor analyzer (Keithley 4200 SCS) and a polarized optical microscope system (CVI Melles Griot and PS-M140T-Modusystems) was used for the measurement of LC-*g*-OFET characteristics.

ASSOCIATED CONTENT

Ⓢ Supporting Information

Performance summary, optical microscope images of the P3HT layer coated on the device substrates and for the broad area of the LC-*g*-OFET device with and without 5CB molecules, video clips for the operation of the present LC-*g*-OFET devices. This material is available free of charge via the Internet at http://pubs.acs.org.

AUTHOR INFORMATION

Corresponding Authors
*E-mail: ykimm@knu.ac.kr. Tel.: +82-53-950-5616 (Y.K.).
*E-mail: khj217@knu.ac.kr (H.K.).

Notes
The authors declare no competing financial interest.

ACKNOWLEDGMENTS

REFERENCES

(1) Allard, S.; Forster, M.; Souharce, B.; Thiem, H.; Scherf, U. Organic Semiconductors for Solution-Processable Field-Effect Transistors. *Angew. Chem., Int. Ed.* **2008**, *47*, 4070−4098.

(2) Ortiz, R. P.; Facchetti, A.; Marks, T. J. High-k Organic, Inorganic, and Hybrid Dielectrics for Low-Voltage Organic Field-Effect Transistors. *Chem. Rev.* **2010**, *110*, 205−239.

(3) Dimitrakopoulos, C. D.; Malenfant, P. R. L. Organic Thin Film Transistors for Large Area Electronics. *Adv. Mater.* **2002**, *14*, 99−117.

(4) Nam, S.; Seo, J.; Park, S.; Lee, S.; Jeong, J.; Lee, H.; Kim, H.; Kim, Y. Hybrid Phototransistors Based on Bulk Heterojunction Films of Poly(3-hexylthiophene) and Zinc Oxide Nanoparticle. *ACS Appl. Mater. Interfaces* **2013**, *5*, 1385−1392.

(5) Minemawari, H.; Yamada, T.; Matsui, H.; Tsutsumi, J.; Haas, S.; Chiba, R.; Kumai, R.; Hasegawa, T. Inkjet Printing of Single-Crystal Films. *Nature* **2011**, *475*, 364−367.

(6) Xie, W.; McGarry, K. A.; Liu, F.; Wu, Y.; Ruden, P. P.; Douglas, C. J.; Frisbie, C. D. High-Mobility Transistors Based on Single Crystals of Isotopically Substituted Rubrene-d^{28}. *J. Phys. Chem. C* **2013**, *117*, 11522−11529.

(7) Caraveo-Frescas, J. A.; Nayak, P. K.; Al-Jawhari, H. A.; Granato, D. B.; Schwingenschlögl, U.; Alshareef, H. N. Record Mobility in Transparent p-Type Tin Monoxide Films and Devices by Phase Engineering. *ACS Nano* **2013**, *7*, 5160−5167.

(8) Radisavljevic, B.; Radenovic, A.; Brivio, J.; Giacometti, V.; Kis, A. Single-layer MoS$_2$ transistors. *Nat. Nanotechnol.* **2011**, *6*, 147−150.

(9) Javey, A.; Guo, J.; Wang, Q.; Lundstrom, M.; Dai, H. Ballistic Carbon Nanotube Field-Effect Transistors. *Nature* **2003**, *424*, 654−657.

(10) Walter, S. R.; Youn, J.; Emery, J. D.; Kewalramani, S.; Hennek, J. W.; Bedzyk, M. J.; Facchetti, A.; Marks, T. J.; Geiger, F. M. In-Situ Probe of Gate Dielectric-Semiconductor Interfacial Order in Organic Transistors: Origin and Control of Large Performance Sensitivities. *J. Am. Chem. Soc.* **2012**, *134*, 11726−11733.

(11) Ukah, N. B.; Granstrom, J.; Gari, R. R. S.; King, G. M.; Guha, S. Low-Operating Voltage and Stable Organic Field-Effect Transistors with Poly(methyl methacrylate) Gate Dielectric Solution Deposited from a High Dipole Moment Solvent. *Appl. Phys. Lett.* **2011**, *99*, 243302.

(12) Veres, J.; Ogier, S. D.; Leeming, S. W.; Cupertino, D. C.; Khaffaf, S. M. Low-k Insulators as the Choice of Dielectrics in Organic Field-Effect Transistors. *Adv. Funct. Mater.* **2003**, *13*, 199−204.

(13) Kalb, W. L.; Mathis, T.; Haas, S.; Stassen, A. F.; Batlogg, B. Organic Small Molecule Field-Effect Transistors with Cytop Gate Dielectric: Eliminating Gate Bias Stress Effects. *Appl. Phys. Lett.* **2007**, *90*, 092104.

(14) Huebler, A. C.; Doetz, F.; Kempa, H.; Katz, H. E.; Bartzsch, M.; Brandt, N.; Henning, I.; Fuegmann, U.; Vaidyanathan, S.; Granstrom, J.; Liu, S.; Sydorenko, A.; Zillger, T.; Schmidt, G.; Preissler, K.; Reichmanis, E.; Eckerle, P.; Richter, F.; Fischer, T.; Hahn, U. Ring Oscillator Fabricated Completely by Means of Mass-Printing Technologies. *Org. Electron.* **2007**, *8*, 480−486.

(15) Veres, J.; Ogier, S.; Lloyd, G.; de Leeuw, D. Gate Insulators in Organic Field-Effect Transistors. *Chem. Mater.* **2004**, *16*, 4543−4555.

(16) Li, J.; Sun, Z.; Yan, F. Solution Processable Low-Voltage Organic Thin Film Transistors with High-k Relaxor Ferroelectric Polymer as Gate Insulator. *Adv. Mater.* **2012**, *24*, 88−93.

(17) Roberts, M. E.; Mannsfeld, S. C. B.; Queraltó, N.; Reese, C.; Locklin, J.; Knolll, W.; Bao, Z. Water-Stable Organic Transistors and Their Application in Chemical and Biological Sensors. *Proc. Natl. Acad. Sci. U. S. A.* **2008**, *105*, 12134−12139.

(18) Kim, S. H.; Yang, S. Y.; Shin, K.; Jeon, H.; Lee, J. W.; Hong, K. P.; Park, C. E. Low-Operating-Voltage Pentacene Field-Effect Transistor with a High-Dielectric-Constant Polymeric Gate Dielectric. *Appl. Phys. Lett.* **2006**, *89*, 183516.

(19) Hisakado, Y.; Kikuchi, H.; Nagamura, T.; Kajiyama, T. Large Electro-Optic Kerr Effect in Polymer-Stabilized Liquid-Crystalline Blue Phases. *Adv. Mater.* **2005**, *17*, 96−98.

(20) Seo, J.; Lee, C.; Han, H.; Lee, S.; Nam, S.; Kim, H.; Lee, J.-H.; Park, S.-Y.; Kang, I.-K.; Kim, Y. Touch Sensors Based on Planar Liquid Crystal-Gated-Organic Field-Effect Transistors. *AIP Adv.* **2014**, *4*, 097109.

(21) Seo, J.; Park, S.; Nam, S.; Kim, H.; Kim, Y. Liquid Crystal-on-Organic Field-Effect Transistor Sensory Devices for Perceptive Sensing of Ultra low Intensity Gas Flow Touch. *Sci. Rep.* **2013**, *3*, 2452.

(22) Kymissis, I. *Organic Field Effect Transistors*; Springer, Manhattan, NY, 2009.

(23) Nam, S.; Kim, J.; Lee, H.; Kim, H.; Ha, C.-S.; Kim, Y. Doping Effect of Organosulfonic Acid in Poly(3-hexylthiophene) Films for Organic Field-Effect Transistors. *ACS Appl. Mater. Interfaces* **2012**, *4*, 1281−1288.

(24) Nam, S.; Ko, Y.-G.; Hahm, S. G.; Park, S.; Seo, J.; Lee, H.; Kim, H.; Ree, M.; Kim, Y. Organic Nonvolatile Memory Transistors with Self-Doped Polymer Energy Well Structures. *NPG Asia Mater.* **2013**, *5*, e33.

(25) Vissenberg, M. C. J. M.; Matters, M. Theory of the Field-Effect Mobility in Amorphous Organic Transistors. *Phys. Rev. B* **1998**, *57*, 12964−12967.

(26) Zaumseil, J. P3HT and Other Polythiophene Field-Effect Transistors. *Adv. Polym. Sci.* **2014**, *265*, 107.